IUST
Iran University of Science and Technology

Iranian Journal of Electrical and Electronic Engineering

Journal Homepage: ijeee.iust.ac.ir

Wideband Electromagnetic Shielding Using Wire-mesh-mounted Chiral Particle Array in Concrete Composite Materials

Ayoub Hamidi*(C.A.), Ahmad Cheldavi*(C.A.) and Asghar Habibnejad Korayem**, *** (C.A.)

Abstract: This paper proposes a structure for concrete composite materials that effectively attenuates transmitted power through the composite slab across a wide frequency range. The proposed structure is practical for electromagnetic interference shielding applications. To assess its effectiveness, the proposed structure has been compared with two other structures: a traditional wire mesh used in reinforced composites and an array of helices, a cutting-edge technique for manufacturing lightweight concretes with significant improvements in shielding properties. The comparison among full-wave simulation results indicates that the proposed method leverages the benefits of both techniques. It achieves a shielding effectiveness exceeding 30 dB from low frequencies up to 8.5 GHz and beyond 55 dB from low frequencies up to 4 GHz. Furthermore, an experimental measurement was conducted to validate the full-wave simulation results. An experimental sample was fabricated according to the simulated proposed structure, and the measured shielding effectiveness confirmed the composite's capability in wideband electromagnetic shielding. Theoretically, the proposed structure can enhance the concrete's mechanical characteristics while improving its shielding effectiveness, making it suitable for designing ultra-high-performance concretes.

Keywords: Composite materials, Electromagnetic interference shielding, Helical additives, Planar arrays, Wideband shielding, Wire mesh.

1 Introduction

ELECTROMAGNETIC interference (EMI) shielding is a method used to safeguard electronic devices from electromagnetic energy. There are several techniques for constructing a shielded environment, such as lining walls with aluminum foil or using steel chambers. Recently, shielded buildings are being developed worldwide for various purposes [1]-[9]. In modern construction, particle-loaded concrete is increasingly being used instead of traditional concrete. This cement-based composite can significantly diminish transmitted electromagnetic power and provide shielding against electromagnetic waves while enhancing the mechanical properties of the structure. Both macroscopic and microscopic particles can be integrated into the composite to achieve these goals [10]-[22]. In general, the electromagnetic shielding phenomenon is caused by an impedance mismatch between the incident wave and the intrinsic impedance of the material of which the slab is made. This impedance mismatch may occur in various methods. In terms of adding metallic inclusions to a composite material, the primary physical mechanism is an increase in the effective electrical conductivity of the composite material because of metallic additives. This phenomenon leads to a significant rise in the reflected power from the composite slab. Another mechanism that

Iranian Journal of Electrical & Electronic Engineering, 2024.
Paper first received 09 August 2024 and accepted 26 August 2024.
* The authors are with the School of Electrical Engineering, Iran University of Science and Technology, Tehran 13114-16846, Iran.
E-mails: ayoub_hamidi@cmps2.iust.ac.ir, cheldavi@iust.ac.ir.
** The author is with the School of Civil Engineering, Iran University of Science and Technology, Tehran 13114-16846, Iran
*** The author is with the Department of Civil Engineering, Monash University, Melbourne, VIC, 3800, Australia.
E-mail: ahkorayem@iust.ac.ir.
Corresponding Authors: A Hamidi, A Cheldavi, AH Korayem.

may occur is power loss. In certain conditions, when the host material of the composite or other additives is lossy, the multi-reflections and multi-scatterings inside the composite slab among metallic particles can result in notable power loss. Even though the analysis of these mechanisms is complex, they have been widely studied in recent years for diverse applications [23]-[25]. However, in most cases, reflection is the dominant mechanism.

Different additives are used in designing composites for EMI shielding applications [10]-[22],[26]-[32]. Carbon-based additives have also been mixed into a cement matrix to create a durable slab for EMI shielding [13]-[21]. Steel fibers are another type of additive implemented in a cement matrix [22]. In another study, nickel filaments were incorporated into the design of shielding composites [27]-[29]. More recently, carbon nanofibers have been used for similar purposes [30]-[32].

However, many of these studies are not suitable for application across a wide frequency range, presenting a limitation that needs further investigation. Additionally, the mechanical properties of concrete are essential from various perspectives. Macroscopic additives are more effective than microscopic additives in protecting concrete composites against larger cracks. Furthermore, macroscopic additives are more industrially feasible and have proven effective through empirical testing because achieving a uniform dispersion of nanoparticles in the composite is challenging and remains an active area of research. The proposed structure can improve the mechanical properties of the concrete composite, significantly enhancing its ductility. Additionally, it can be combined with microscopic additives. Using the proposed method in conjunction with nanoparticles is advantageous and can be applied in designing ultra-high-performance concrete (UHPC) [33], [34].

Macroscopic conductive additives can be incorporated into concrete in various shapes and sizes. Helical-shaped particles are a well-known type of chiral inclusion used for electromagnetic interference (EMI) shielding applications, particularly due to their resonant properties [35]-[39]. These additives can be arranged in an array or distributed randomly, with each method having advantages and disadvantages. We prefer arranging them in the form of an array to maximize their potential to increase shielding effectiveness across a wide frequency range or improve different characteristics of composite materials. Namely, utilizing an array of chiral particles in a concrete host medium results in a lightweight concrete composite material with enhanced shielding effectiveness, making it suitable for EMI shielding applications [40]. Moreover, new techniques have recently emerged for organizing the conductive particles in concrete paste [41]-[43].

On the other hand, using wire mesh to construct reinforced concrete is a traditional technique. This composite structure can effectively attenuate transmitted electromagnetic power through the reinforced slab, specifically in the low-frequency range. The shielding effectiveness of a wire mesh has been extensively studied and mathematically analyzed in the past [44]-[51]. However, its restricted ability in electromagnetic shielding, which is effective only in the low-frequency range, limits its usage in EMI shielding applications, especially in concrete composite designs.

This paper introduces a novel structure for concrete composite materials for electromagnetic interference (EMI) shielding applications. The structure features an array of helical-shaped conductive particles as chiral additives mounted on wire mesh embedded in a concrete material as the host medium. This design combines the benefits of both wire mesh and chiral particles, providing significant shielding effectiveness over a wide frequency range. In certain cases, the helical particles can replicate the behavior of a below-cutoff cylindrical waveguide, leading to a significant decrease in transmitted power from the array of helical particles within its resonance frequency range. The wire mesh not only shields the low-frequency range but also acts as a short circuit termination at the end of the aforementioned cylindrical waveguide, substantially enhancing the shielding effectiveness across a wide frequency range.

This paper is organized into four sections. Section 2 introduces three composite structures prepared for investigation using full-wave simulations, comprising four sub-sections. The first sub-section introduces the wire mesh structure, the second details an array of helices structure, and the third presents the proposed structure, which includes a wire-mesh-mounted array of helices. The fourth sub-section provides the results and discussion of the full-wave simulations for all structures. Section 3 focuses on validating the full-wave simulations with experimental measurements. Finally, Section 4 concludes the paper and highlights the key findings of this study.

2 Three Composite Structures Preparation for Full-Wave Simulations

2.1 Wire mesh

The first structure involves implementing metal wire meshes embedded in the concrete paste, a traditional method for constructing reinforced concrete composites. Furthermore, it is a prevalent structure for shielding against electromagnetic power and can be used in concrete composites in some applications. A wire mesh is shown in Fig. 1(a). The shielding properties of this structure, along with similar structures or metamaterials,

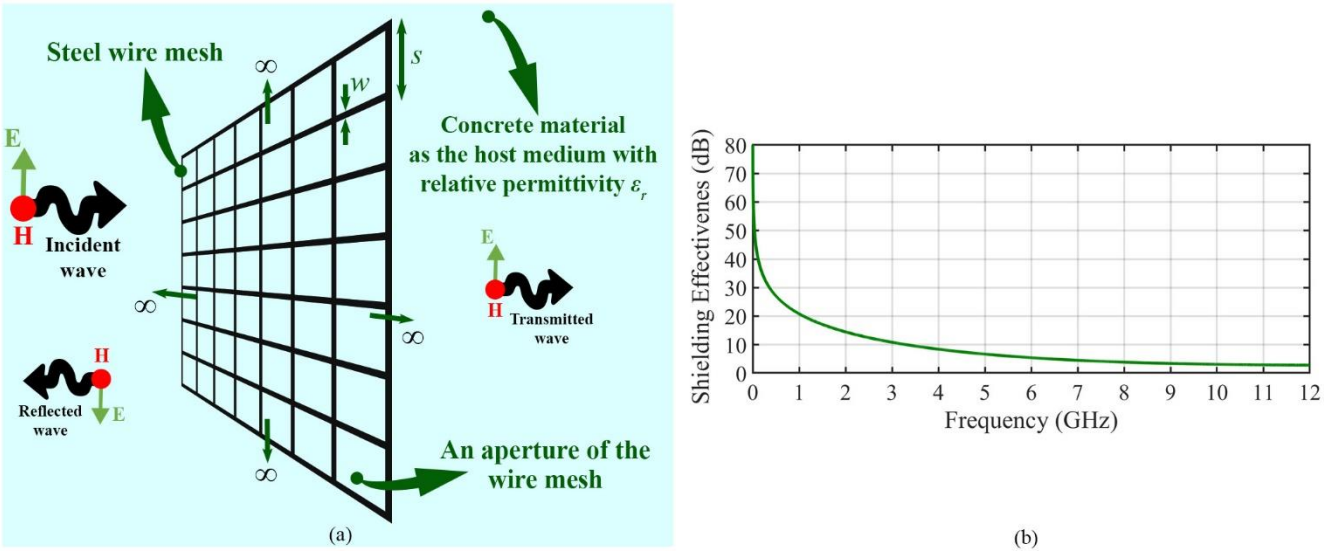

Fig. 1 (a) A wire mesh embedded in an infinite medium of the host material. In this work, the host material, which is represented in blue, is concrete. (b) The shielding effectiveness of the wire mesh shown in (a).

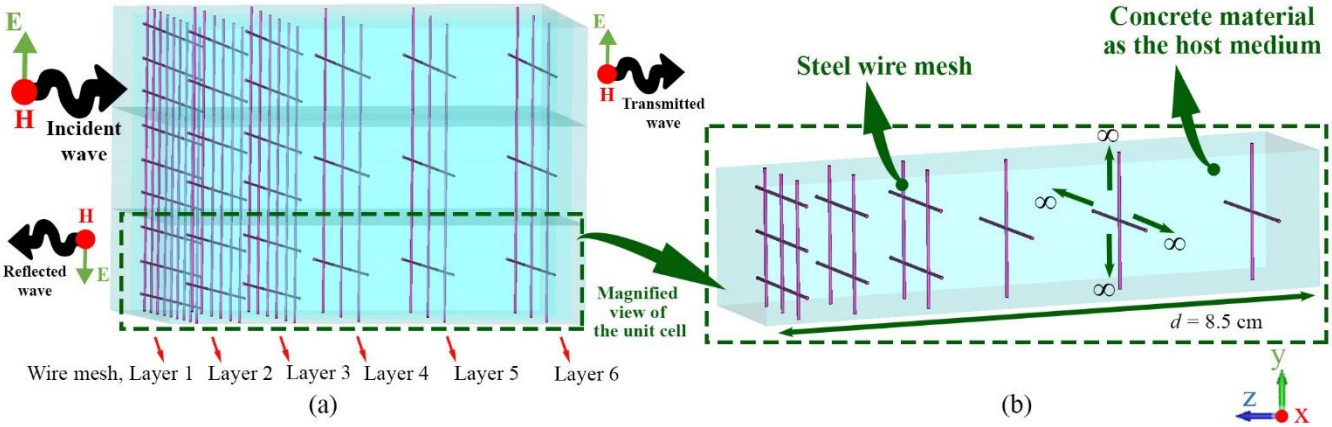

Fig. 2 (a) Six-layer wire meshes embedded in the concrete material as the host medium, together forming a concrete composite slab with infinite cross-section. (b) The unit cell of the structure.

have been extensively studied and mathematically analyzed [44]-[51]. These analytical methods provide insights into the behavior of a wire mesh within a concrete host medium.

The shielding effectiveness parameter is usually denoted by the symbol *SE* and can be expressed as Eq. (1). In this context, *Pi* represents the power of the incident wave traveling toward the interface or slab, and *Pt* denotes the power of the transmitted wave traveling outward the interface or slab, illustrated in Figs. 1(a).

$$SE^{(\mathrm{dB})} = 10\log\left(\frac{P_i}{P_t}\right) \tag{1}$$

The shielding effectiveness (*SE*) of a wire mesh illuminated by a TEM plane wave, as shown in Fig. 1(a), can be expressed as Eq. (1) [47].

$$SE = R + A + B + k_1 + k_2 + k_3 \tag{2}$$

Where R is the reflection loss related to the meshed screen, A is the attenuation corresponding to an aperture (a square made of metal wire) as a waveguide below cutoff, B is the multiple reflection correction factor, k_1 accounts for the various number of similar apertures per unit area, k_2 accounts for the loss due to skin depth, and k_3 accounts for the coupling between adjacent apertures. The reflection loss R can be determined by

$$R = 20\log\left(\frac{1+k^2}{4k}\right) \tag{3}$$

where k is expressed as

$$k = 6.69\sqrt{\varepsilon_r}\, fs \times 10^{-9} \tag{4}$$

In Eq. (4), f is the frequency of the incident wave, s is the width of the square aperture or the size of the wire spacing as shown in Fig. 1(a), and ε_r is the relative electric permittivity of the host medium, which is the concrete material. The attenuation loss A and multiple reflections correction factor B should be respectively

Table 1. The wire mesh's specifications of each layer.

Wire mesh layer number	Size of the aperture "s" (mm)	Metal wire diameter "w" (mm)
Layer 1	25	0.3
Layer 2	25	0.3
Layer 3	25	0.3
Layer 4	12	0.3
Layer 5	12	0.3
Layer 6	8	0.3

derived by Eq. (5) and Eq. (6).

$$A = 27.3t/s \tag{5}$$

$$B = 20\log\left(1+\left(\frac{k-1}{k+1}\right)^2 10^{-0.1A}\right) \tag{6}$$

In Eq. (5), t is the depth of the square aperture. Additionally, the factors k1, k2, and k3 are expressed as Eq. (7), Eq. (8), and Eq. (9) respectively [47].

$$k_1 = -10\log(a \times n) \tag{7}$$

$$k_2 = -20\log\left(1+35(w/\delta)^{-2.3}\right) \tag{8}$$

$$k_3 = 20\log\left(\cot(A/8.686)\right) \tag{9}$$

where a is the area of each aperture in cm^2, n is the number of the wire mesh's unit cells per square centimeter, w is the metal wire's diameter, and δ is the skin depth for the metal the wire mesh is made of.

Figure 1(b) shows the shielding effectiveness of a single-layer wire mesh embedded in an infinite medium made of concrete material, as illustrated in Fig. 1(a), with $s = 5$ mm and $w = 0.3$ mm. these values for the shielding effectiveness have been obtained by Eq. (2). Generally, Fig. 1(b) demonstrates that the wire mesh attenuates the transmitted power at low frequencies based on the mesh size. In the very low-frequency range, the wavelength is much larger than the mesh size, allowing it to attenuate the transmitted power; however, as the frequency increases, its shielding effectiveness significantly decreases. From the perspective of frequency selective surfaces (FSS), it functions as a high-pass FSS [52].

A multi-layer structure can be implemented to increase the shielding effectiveness utilizing wire mesh. Figure 2(a) illustrates six parallel wire meshes that make a six-layer structure. The unit cell of this structure can be observed in Fig. 2(b). The cross-section of the slab and the wire meshes is infinite. It is assumed that an incident TEM plane wave propagates toward a concrete slab, including wire meshes along the -z-axis. This structure was simulated using CST Studio Suite software, and the results will be presented in Section 2.D. In the full-wave simulation, the reinforced concrete slab has a thickness of 8.5 cm, as depicted in Fig. 2(b). Table 1 lists the geometric parameters of each wire mesh.

2.2 Array of helices

The second structure features an array of helices as chiral particles embedded in a concrete slab, forming a composite material. Metamaterials, chiral particles, and chiral media are utilized for EMI shielding applications [52]. For instance, a multi-layer array of chiral particles can be employed to achieve high shielding effectiveness while also designing a lightweight composite material [40]. However, designing a wideband structure is a significant challenge. To address this, the helical particles in each layer vary in size, broadening the applicable bandwidth.

This design leverages the resonant properties of an infinite periodic planar array of helical particles to effectively attenuate transmitted electromagnetic power, making it suitable for EMI shielding applications. Theoretically, the strong attenuation of transmitted power from infinite periodic arrays of helical particles, as shown in Fig. 3(c), is due to the particles' ability to imitate the TE_{11} mode of a cylindrical waveguide and the corresponding surface current on the helical wire. This occurs in the resonance frequency range below the TE_{11} mode cutoff frequency of a cylindrical waveguide with a radius similar to that of the helical particle.

Table 2. The particles' specifications of each planar array of helices.

Planar Array Number	Array 1	Array 2	Array 3	Array 4	Array 5	Array 6
Fractional size	1	1.25	1.25^2	1.25^3	1.25^4	1.25^5
R (mm)	3.9	4.9	6.1	7.7	9.6	12
Pitch angle	4.55°	4.55°	4.55°	4.55°	4.55°	4.55°
Number of turns	1.75	1.75	1.75	1.75	1.75	1.75
Axial length (mm)	3.4	4.3	5.4	6.8	8.4	10.5
Wire diameter (mm)	0.16	0.20	0.26	0.32	0.4	0.48
Resonance frequency (GHz)	5.28	4.22	3.38	2.70	2.16	1.73

Figure 3(a) shows an infinite periodic planar array of conductive cylinders (cylindrical waveguides), while Fig. 3(c) illustrates an infinite periodic planar array of seven-turn helices. Figures 3(e)-3(h) compare the electric field configurations on a cross-section of these two planar arrays. Figures 3(e) and 3(g) provide the comparison at 2GHz, which is within the resonance frequency range below the TE_{11} mode cutoff frequency of 3.1 GHz for the cylindrical waveguide. Figures 3(f) and 3(h) show a similar comparison at 3.5 GHz, above the cutoff frequency. These comparisons reveal a considerable similarity in the electric field configurations at different frequencies. Furthermore, Figures 3(i)-3(l) compare the power density on a cross-section perpendicular to the slab and parallel to the incident wave propagation direction.

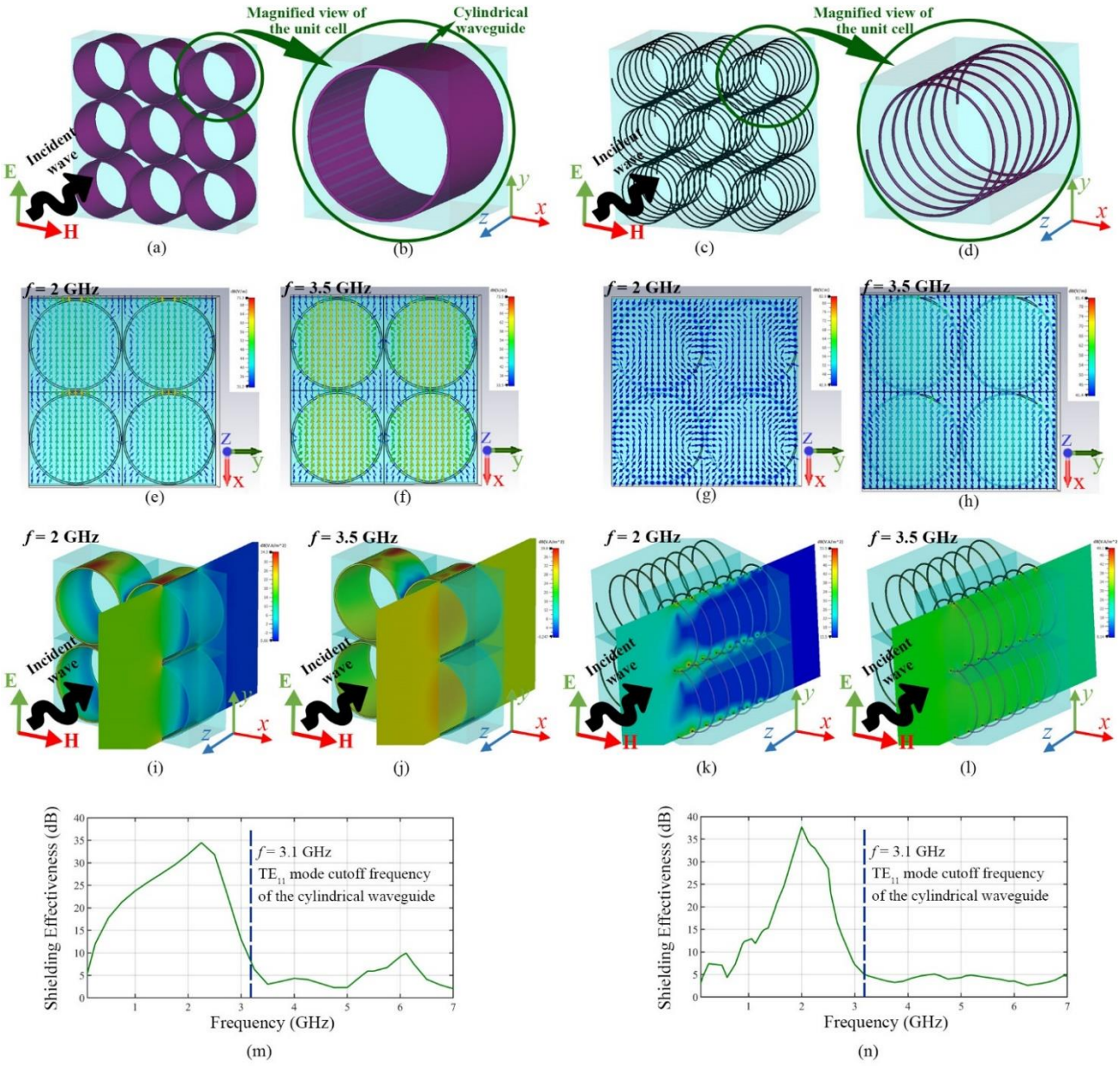

Fig. 3 The similarity between the electric field patterns and the transmitted power of two different planar arrays embedded in a concrete composite: an infinite periodic planar array of conductive cylinders (cylindrical waveguides) (left two columns) and an infinite periodic planar array of seven-turn helices (right two columns), both with identical radii of 12 mm. The TE_{11} mode cutoff frequency of the cylindrical waveguide is 3.1 GHz. The blue transparent cube represents the surrounding concrete material as the host medium. (a) The infinite periodic planar array of conductive cylinders. (b) The unit cell of the array in (a). (c) The infinite periodic planar array of seven-turn helices. (d) The unit cell of the array in (c). (e) The electric field configuration on a cross-section, parallel to the array plane, of the cylinder at 2 GHz, below the cutoff frequency. (f) Similar to (e) at 3.5 GHz, beyond the cutoff frequency. (g) The electric field configuration on a cross-section, parallel to the array plane, of the helix at 2 GHz, below the cutoff frequency. (h) Similar to (g) at 3.5 GHz, beyond the cutoff frequency. The electric field configuration of the TE_{11} mode can be observed in the helix array in (g) and (h), which is analogous to the array of cylindrical waveguides in (e) and (f). (i) The time-average power density contour on a cross-section, perpendicular to the array plane, of the cylinders at 2 GHz, below the cutoff frequency. (j) The time-average power density contour on a cross-section, perpendicular to the array plane, of the cylinders at 3.5 GHz, beyond the cutoff frequency. (k) Similar to (i) for the array of helices. A significant attenuation of the transmitted wave can be observed in (i) and (k). (l) Similar to (j) for the array of helices. A considerable transmission can be observed in (j) and (l). (m) The shielding effectiveness of the infinite periodic planar array of conductive cylinders, shown in (a), obtained by full-wave simulation. (n) The shielding effectiveness of the infinite periodic planar array of seven-turn helices, shown in (c), obtained by full-wave simulation.

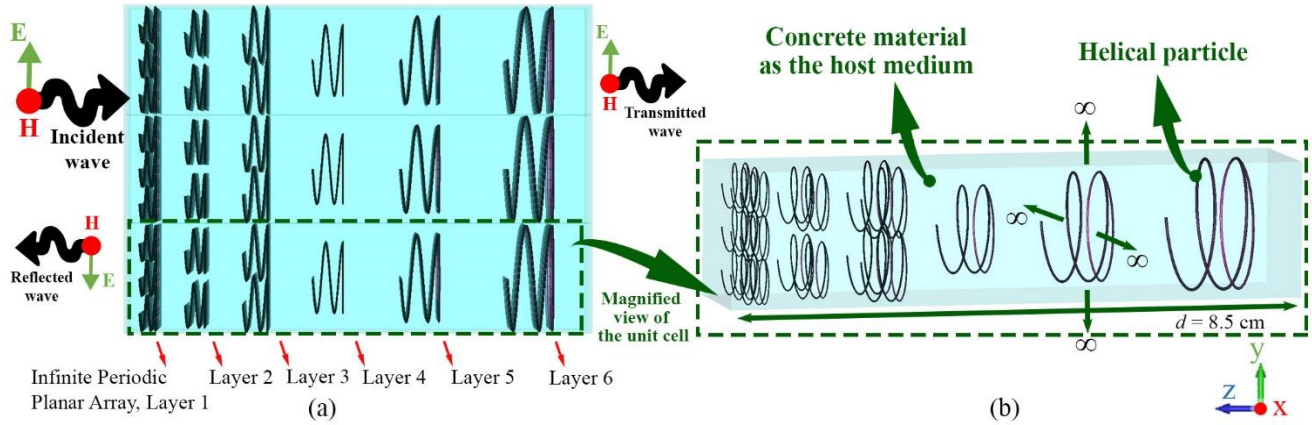

Fig. 4 An array of helical particles including six parallel infinite periodic planar arrays of helices embedded in a concrete material as the host medium, together forming a concrete composite slab with infinite cross-section. (b) The unit cell of the structure.

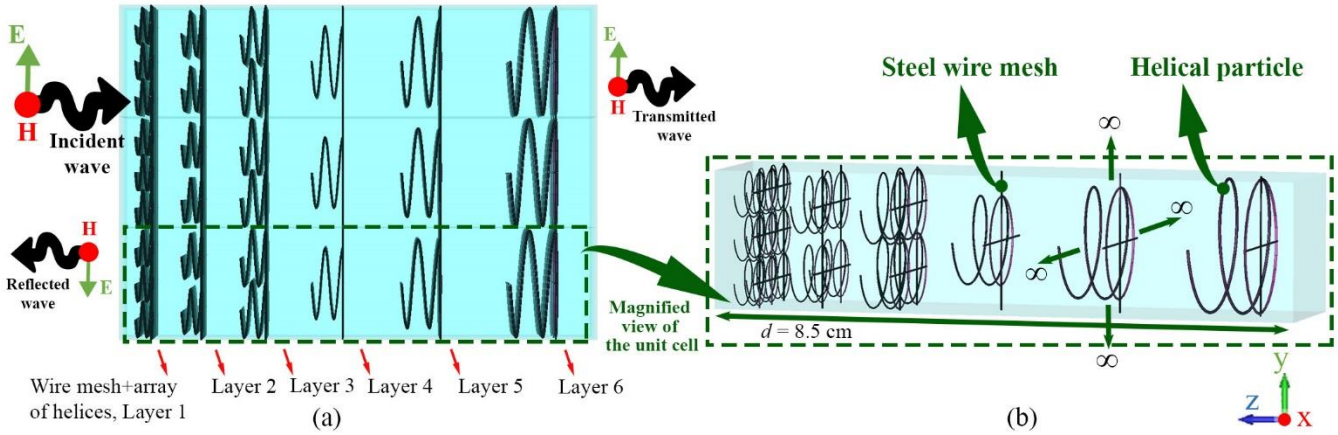

Fig. 5 An array of helical particles, including six parallel infinite periodic planar arrays of helices mounted on wire meshes, which are embedded in a concrete material as the host medium, together forming a concrete composite slab with infinite cross-section. (b) The unit cell of the structure.

The comparison highlights significant shielding properties for both planar arrays at 2 GH, as shown in Figs. 3(i) and 3(k), while also indicating notable power transmission through both arrays at 3.5 GHz. Figures 3(m) and 3(n) illustrate the shielding effectiveness of both planar arrays as obtained from full-wave simulations, highlighting the similar behavior of both arrays. From the perspective of frequency selective surfaces (FSS), the array of helices operates as a band-stop FSS [52].

The scattering of an individual chiral particle or canonical helix is maximized when the wavelength is approximately equal to the particle's circumference [37]. The resonance frequency of a helix-loaded composite occurs at a wavelength equal to 0.75 times the total length of the helix wire, which is almost the same as the circumference of the helix in particles with a small number of turns and pitch angle [38],[39]. Similarly, for an infinite periodic planar array of helical particles with a slight pitch angle and few turns, such as one of the planar arrays in the six-layer structure shown in Fig. 4(a), the central frequency of the resonant band is the frequency whose wavelength is roughly equal to the helical particle's circumference within the unit cell of the planar array.

Given our design objectives, we use a 6-layer structure consisting of six parallel infinite periodic planar arrays, which are dense enough, as shown in Fig. 4(a). All planar arrays are embedded in concrete as the host medium.

The elements within each planar array have identical orientation and geometry, but the arrays can vary in element and unit cell size. Different unit cell sizes are selected to achieve a wideband structure. In this example, the particle and unit cell size in each planar array is scaled from the previous array. We aim to design an array of helical particles for shielding applications in the frequency range of 2-4 GHz. Thus, the largest particle (layer 6) and the second smallest particle (layer 2) are designed in such a way that the center of their resonance bands occur at 1.7 GHz and 4.2 GHz, respectively. Additionally, an extra layer (layer 1)

with a smaller particle size and higher resonance frequency (5.2 GHz) is included to enhance performance within the desired frequency band.

The distances between the arrays are assumed to be arbitrary and dependent on the specific utility and design requirements. In this study, we design and simulate one 6-layer array of helical particles using the full-wave simulation software CST Studio Suite. The composite slab has a thickness of 8.5 cm, as shown in Fig. 4(b). The geometric parameters were determined through a parametric study. Specifically, the number of turns should be an odd multiple of a quarter-turn (1.75 turns) to achieve a bi-anisotropic slab capable of effectively interacting with two orthogonal polarizations of the incident wave's electric field. Additionally, a ring was added to the end of the helical particles to enhance the practicality of the structure and facilitate its realization. Table 2 presents the specifications of the helical particles' geometry for each array.

2.3 Array of helices mounted on wire meshes

Table 3. The materials' characteristics in the full-wave simulations.

Material	Quantity	Value
Concrete	ε_r	Dispersive, Complex, and 1st order model 5.5-0.2i at f=1.36 GHz 5.5-0.12i at f=2.52 GHz 5.55-0.09i at f=3.68 GHz
	μ_r	1
steel	ε_r	1
	μ_r	2000
	σ	1.03e+07 (S/m)

The third and proposed structure combines the first two designs. It incorporates a multi-layer array of helices, where each planar array of helices is mounted on a wire mesh. The size of the wire mesh apertures (wire spacing) in each layer matches the unit cell size of its corresponding planar array of helices. Figure 5 illustrates the proposed structure and its unit cell. We simulated and assessed this 6-layer structure using the full-wave simulation software CST Studio Suite. The geometric parameters of the helical particles and the wire mesh are identical to those specified in Sections 2.A and 2.B, as detailed in Tables 1 and 2.

Theoretically, the wire mesh acts as a short circuit termination for the cylindrical waveguides imitated by the helical particles. This significantly enhances the slab's shielding effectiveness, even at the operational frequency of the helix array.

Mounting the planar array of helices on a wire mesh also facilitates the production of concrete composites with embedded helical arrays, which otherwise face manufacturing challenges. This proposed structure not only mitigates these manufacturing difficulties but also ensures better distribution of the helical particles within the host medium of the composite material. The uniform distribution of the additives is a crucial factor in the composite material's mechanical characteristics and electromagnetic shielding properties.

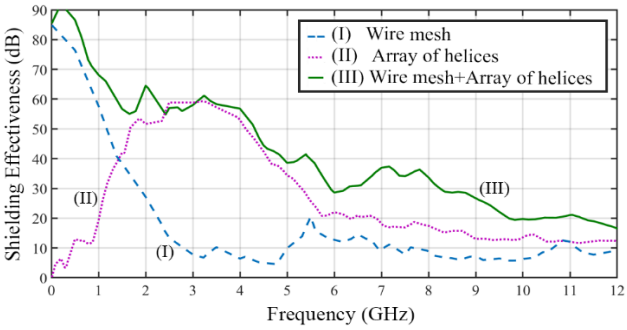

Fig. 6 The shielding effectiveness of concrete composites reinforced by three different structures, each with a thickness of 8.5 cm obtained by full-wave simulations.

2.4 Results and Discussion

The shielding effectiveness of the three structures presented in Sections 2.A, 2.B, and 2.C were evaluated by full-wave simulations in CST Studio Suite software. In the software, full structures cannot be simulated due to the infinite cross-section of the slabs; instead, a unit cell approach with periodic boundary conditions is used. The unit cell of these three structures can be observed in Figs. 2(b), 4(b), and 5(b) respectively. Two ports are placed on either side of the slab. Port 1 is excited, and the total power delivered to Port 2 is measured. Shielding effectiveness is calculated using Eq. (1). A Floquet port is implemented to excite the unit cell, and the frequency domain solver utilizes the Method of Moments (MoM) for simulation. Moreover, Table 3 presents the characteristics of the materials used in all simulations, as recorded in the software database.

Figure 6 compares the shielding effectiveness of concrete composites reinforced by three different structures, each with a thickness of 8.5 cm. For the first structure, which employs wire mesh, line graph (1) shows that the shielding effectiveness is significantly high at low frequencies but decreases considerably as the frequency increases. This trend is consistent with the mathematical analysis results for a single-layer wire mesh shown in Figure 1(b).

Table 4. Shielding effectiveness (SE) of structures with macroscopic additives

Type of Additives	Slab Thickness (cm)	Additives Volume Fraction	SE (dB) at f =1.5 GHz	SE (dB) at f =3.5 GHz	References
Wire mesh (single layer)	2.5	0.15%	4	3.3	[47],[48]
Randomly distributed rods	2.5	2.4%	16	28	[40]
Multi-layer array of helices	11	0.1%	23	44	[40]
Multi-layer array of helices with end ring	8.5	0.3%	41	57	This study
Proposed structure	8.5	0.4%	57	58	This study

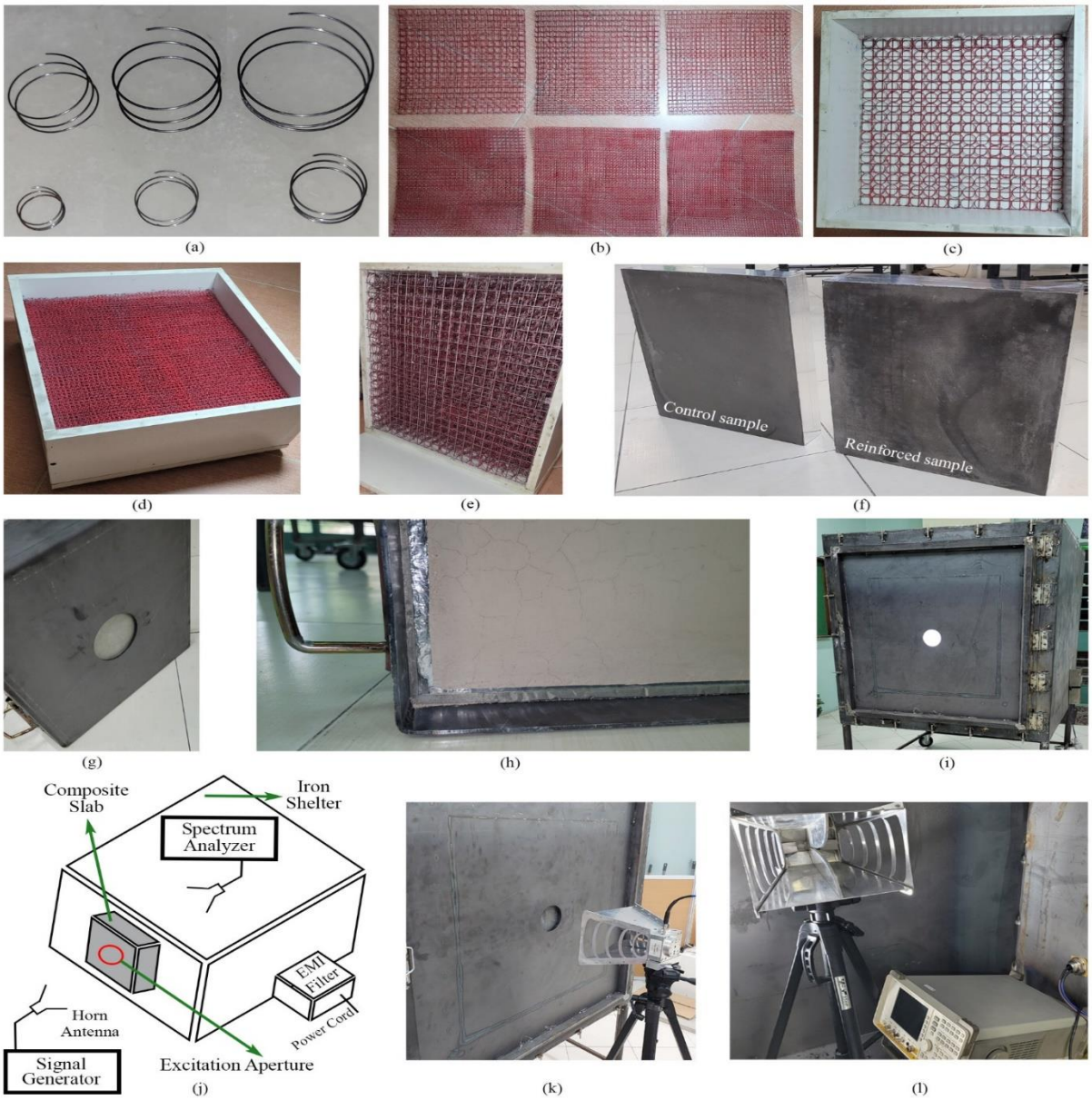

Fig. 7 (a) six different helical steel particles. (b) Six planar arrays of helices mounted on wire meshes. (c) securing the sixth layer in its position within the mold. (d) six layers fixed in their position within the mold. (e) Back view of the proposed structure in the mold before pouring the concrete paste. (f) The reinforced (with steel additives) and the control (without steel additives) samples after the drying process. (g) Preparing a slab in a holder for mounting in the test setup. (h) putting gaskets around the samples in the holder for mounting in the test setup. (i) The iron shelter. (j) The test setup. (k) The horn antenna, which illuminates the electromagnetic incident wave toward the concrete composite slab. (l) The horn antenna and spectrum analyzer in the iron shelter.

Line graph (2) illustrates the shielding effectiveness for the second structure, which includes only an array of helices. It indicates very low attenuation of transmitted power at low frequencies. However, notable shielding effectiveness is observed between approximately 1.5 and 5.5 GHz, with values exceeding 30 dB and peaking at around 60 dB in the 2.5 to 3.5 GHz range, indicating substantial attenuation.

Line graph (3) depicts the shielding effectiveness of the proposed structure, which combines an array of helices mounted on six-layer wire meshes. This graph shows a significant improvement compared to the first and second structures, which use only wire mesh or an array of helices alone. The proposed structure notably enhances the shielding property, especially within the resonance frequency range of the helical particle array. Significant attenuation is achieved over a wide frequency range, with shielding effectiveness exceeding 30 dB from low frequencies up to 8.5 GHz and beyond 55 dB from low frequencies up to 4 GHz. These results demonstrate that the proposed structure can substantially attenuate transmitted power through the composite slab across a broad frequency range.

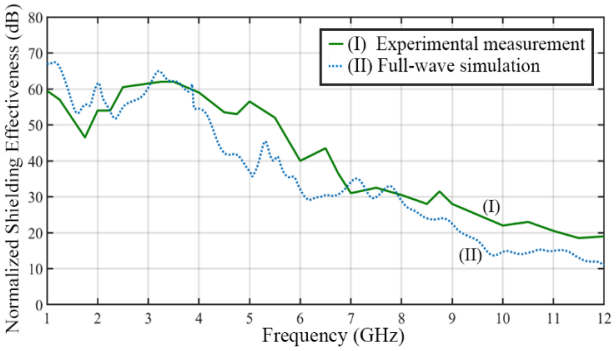

Fig. 8 A comparison between the normalized shielding effectiveness of the proposed structure derived by full-wave simulation and experimental measurement. This figure illustrates the difference in shielding effectiveness between the reinforced sample (containing the array of steel helices mounted on wire meshes) and the control sample (without any steel additives) for both the full-wave simulation and the experimental measurement.

In terms of shielding properties, the helix-loaded composites significantly outperform conventional EMI shielding structures, including metallic wire meshes and randomly distributed rods [7],[40],[47],[48]. Table IV compares these structures, all utilizing macroscopic additives at various additive volume fractions (the ratio of the metallic additives' volume to that of the composite) embedded within concrete material. The comparison reveals that helical-based composites can achieve high levels of shielding effectiveness with lower additive volumes [40].

It should be noted that there are no significant restrictions on the thickness of the proposed structure to achieve this level of shielding effectiveness. The thickness of the slab can be reduced by decreasing the pitch angle (or spacing between turns) of the helix particles or the space between different layers of the array. These changes will reduce the thickness of the proposed structure without a noticeable decrease in its shielding properties across the same frequency band, which is one of the advantages of this structure.

3 Validation with Experimental Measurement

An experimental measurement was conducted to validate the results of the full-wave simulation for the proposed structure, described in Section 2.C. We manufactured a reinforced concrete composite sample with cross-sectional dimensions of 40×40 cm^2 and a slab thickness of 8.5 cm. This thickness was selected to match the simulated samples. Additionally, we attempted to ensure that the geometry and size of the helical particles and wire meshes in the experimental sample matched those used in the full-wave simulations for the proposed structure, as detailed in Tables 1 and 2. All components were made of steel. Figure 7(a) shows the six different helical particles corresponding to each layer (planar array). To fabricate the reinforced concrete composite, the helical particles for each of the six layers were mounted on their respective wire meshes and fixed using red spray adhesive. These six planar arrays of helices mounted on wire meshes are shown in Fig 7(b). In the second step, each layer was secured in its position within a mold, as illustrated in Figs. 7(c)-7(e). Then, the concrete paste was poured into the mold.

Two samples were prepared: one reinforced with helical steel additives and wire meshes, and one control sample without any conductive additives. Both samples had dimensions of 40×40×8.5 cm^3, as depicted in Figure 7(f). After the drying process, the shielding effectiveness of both slabs was measured using the iron shelter and the test setup shown in Fig. 7(i) and Fig. 7(j), respectively. Measurements were taken across a frequency range from 1 to 12 GHz in 0.25 GHz intervals.

The transmitted power through control samples (samples without the array of helices or wire mesh) differs between experimental measurements and full-wave simulations due to slight variations in the concrete material's behavior in each method. To eliminate the effect of the concrete material on the shielding effectiveness of the composites in both experimental measurements and full-wave simulations, control samples were used. The normalized shielding effectiveness (SE_N) of the reinforced sample is the

difference between its shielding effectiveness and the control sample's shielding effectiveness, calculated by Equation (8).

$$SE_N = SE_{\text{Reinforced sample}}(\text{dB}) - SE_{\text{Control sample}}(\text{dB}) \quad (10)$$

Figure 8 compares the normalized shielding effectiveness of the proposed structure obtained from the experimental measurement and the full-wave simulation. It indicates that the full-wave simulation results align with the experimental measurements, suggesting that the structure can significantly attenuate the transmitted power through the concrete composite slab across a wide frequency range.

4 Conclusion and Highlights

In conclusion, utilizing an array of helical particles mounted on wire meshes in a composite material leverages the advantages of both structures: the array of helices and the wire meshes. The wire mesh can shield against low-frequency incident waves, while the helical particle array operates in a higher frequency range where the wire mesh alone cannot provide sufficient shielding effectiveness. The key findings of this paper can be highlighted as follows:

- Low-Frequency Shielding: Wire mesh exhibits significant electromagnetic shielding effectiveness in the low-frequency range, functioning as a high-pass frequency selective surface (FSS).
- Limitations of Wire Mesh: Although wire mesh is commonly used in the production of reinforced concretes, its limited bandwidth restricts its effectiveness for wideband electromagnetic shielding applications.
- Helical Particles' Resonance: The helical particles' ability to imitate the dominant mode of a cylindrical waveguide and the corresponding surface current on the helical wire results in a strong attenuation of transmitted power from infinite periodic arrays of helices.
- Band-Stop FSS Functionality: An array of helical particles can effectively attenuate transmitted power through the composite slab within its resonance frequency range, which lies below the dominant mode cutoff frequency of a cylindrical waveguide with a radius similar to that of the helical particle. In terms of FSS, it functions as a band-stop filter.
- Wideband Shielding: The combination of helical particle arrays mounted on wire meshes in a composite material offers significant shielding effectiveness across a wide frequency range. This proposed structure is suitable for EMI shielding applications and also facilitates the industrial application of helical arrays within concrete.
- Multilayer Structure Benefits: Implementing a multilayer structure enhances the engineering of composites, helping to achieve specific design objectives.

Beyond improving electromagnetic shielding, the proposed structure can also enhance the mechanical properties of concrete, making it an ideal candidate for the development of ultra-high-performance concretes.

References

[1] M. Mardiguian and J. P. Caron-Fellens, "The intelligent concrete: A new, economical technique for architectural shielding of buildings," *IEEE Electromagn. Compat. Mag.*, vol 6, no 2, pp. 50-54, Jul. 2017.

[2] S. Quintana *et al.*, "Design and operation of a real-scale electromagnetic shielding evaluation system for reinforced composite construction materials," *J. Mater. Civ. Eng.*, vol 30, no 8, Aug. 2018, Art. no. 04018162.

[3] S. Keykavous-Amand, and R. Peymanfar, "Fabrication of clay soil/CuFe2O4 nanocomposite toward improving energy and shielding efficiency of buildings," *Sci. Rep.*, vol. 11, no. 1, Oct 2021, Art. no. 20832.

[4] R. Peymanfar, S. Keykavous-Amand, M. M. Abadi, and Y. Yassi, "A novel approach toward reducing energy consumption and promoting electromagnetic interference shielding efficiency in the buildings using Brick/polyaniline nanocomposite," *Construction Building Mater.*, vol. 263, Dec. 2020, Art. no. 120042.

[5] 5D. Johns, "Designing building structures for protection against EMP and lightning," *IEEE Electromagn. Compat. Mag.*, vol. 5, no. 1, pp. 50-58 May 2016.

[6] J. Roberts, Kenneth Lee Ford, and Jonathan M. Rigelsford, "Secure electromagnetic buildings using slow phase-switching frequency-selective surfaces," *IEEE Trans. Antennas Propag.*, vol. 64, no. 1, pp. 251-261, Nov. 2015.

[7] S. Y. Hyun et al., "Analysis of shielding effectiveness of reinforced concrete against high-altitude electromagnetic pulse," IEEE Trans. Electromagn. Compat., vol. 56, no. 6, pp. 1488-1496, May 2014.

[8] Nguyen, Lim, Aaron Krause, Christopher Tuan, Joel D. Blasey, James P. Zemotel, Holly McNerney, and Ferdinand J. Metzger. "Shielding effectiveness

performance of conductive concrete structures." In IEEE Int. Symp. Electromagn. Compat. Signal/Power Integrity (EMCSI), Washington, DC, USA, 2017, pp. 360-363.

[9] P. Ängskog *et al.*, "Shielding effectiveness and HPM vulnerability of energy-saving windows and window panes," *IEEE Trans. Electromagn. Compat.*, vol. 61, no. 3, pp. 870-877, May 2018.

[10] T. Khalid, L. Albasha, N. Qaddoumi, and S. Yehia, "Feasibility study of using electrically conductive concrete for electromagnetic shielding applications as a substitute for carbon-laced polyurethane absorbers in anechoic chambers," *IEEE Trans. Antennas Propag.*, vol. 65, no. 5, pp. 2428-2435, Feb. 2017.

[11] D. Wanasinghe, F. Aslani, and G. Ma, "Electromagnetic shielding properties of carbon fibre reinforced cementitious composites," *Construction Building Mater.*, vol. 260, Nov. 2020. Art. no. 120439.

[12] Z. Liu, H. Ge, J. Wu, and J. Chen, "Enhanced electromagnetic interference shielding of carbon fiber/cement composites by adding ferroferric oxide nanoparticles," *J. Construction Building Mater.*, vol. 151, pp. 575-581 Oct. 2017.

[13] D. Micheli, R. Pastore, A. Vricella, R. B. Morles, M. Marchetti, A. Delfini, F. Moglie, and V. M. Primiani, "Electromagnetic characterization and shielding effectiveness of concrete composite reinforced with carbon nanotubes in the mobile phones frequency band," *J. Mater. Sci. Eng.: B*, vol. 188, pp. 119-129, Oct. 2014.

[14] A. P. Singh, B. K. Gupta, M. Mishra, A. Chandra, R. B. Mathur, and S. K. Dhawan, "Multiwalled carbon nanotube/cement composites with exceptional electromagnetic interference shielding properties," *J. Carbon*, vol. 56, pp. 86-96, May 2013.

[15] I. W. Nam, H. K. Kim, and H. K. Lee, "Influence of silica fume additions on electromagnetic interference shielding effectiveness of multi-walled carbon nanotube/cement composites," *J. Construction Building Mater.*, vol. 30, pp. 480-487, May 2012.

[16] J. Chen, D. Zhao, H. Ge, and J. Wang, "Graphene oxide-deposited carbon fiber/cement composites for electromagnetic interference shielding application," *J. Construction Building mater.*, vol. 84, pp. 66-72, Jun. 2015.

[17] A. P. Singh, M. Mishra, A. Chandra, and S. K. Dhawan, "Graphene oxide/ferrofluid/cement composites for electromagnetic interference shielding application," *J. Nanotech.*, vol. 22, no. 46, Oct. 2011, Art. no. 465701.

[18] J. Cao, and D. D. L. Chung, "Colloidal graphite as an admixture in cement and as a coating on cement for electromagnetic interference shielding," *J. Cement Concrete Res., vol. 33, no. 11*, pp. 1737-1740, Nov. 2003.

[19] J. M. Chiou, Z. Qijun, and D. D. L. Chung, "Electromagnetic interference shielding by carbon fibre reinforced cement," *J. Composites*, vol. 20, no. 4, pp. 379-381, Jul. 1989.

[20] X. Fu and D. D. L. Chung, "Submicron carbon filament cement-matrix composites for electromagnetic interference shielding," *J. Cement Concrete Res.*, vol. 26, no. 10, pp. 1467-1472, Oct. 1996.

[21] X. Fu and D. D. L. Chung, "Submicron-diameter-carbon filament cement-matrix composites," *J. Carbon*, vol. 36, no. 4, pp. 459-462, Jan 1998.

[22] S. Wen and D. D. L. Chung, "Electromagnetic interference shielding reaching 70 dB in steel fiber cement," *J. Cement Concrete Res.*, vol. 34, no. 2, pp. 329-332, Feb. 2004.

[23] A. N. Moqadam, A. Pourziad, and S. Nikmehr. "Motion of small spherical particles in an arbitrary oriented cluster due to the microwave propagation," *Prog. Electromagn. Res. B*, vol. 76, pp. 97-110, Jun. 2017.

[24] M. I. Mishchenko, L. D. Travis, and D. W. Mackowski. "T-matrix computations of light scattering by nonspherical particles: A review," *J. Quantitative Spectrosc. Radiat. Transf.*, vol 55, no. 5, pp. 535-575, May 1996.

[25] A. N. Moqadam, A. Pourziad, and S. Nikmehr. "Radiation Forces on a Cluster of Spherical Nanoparticles in Visible Light Spectrum," *Prog. Electromagn. Res. C*, vol. 75, pp. 99-109, jun. 2017.

[26] D. D. L. Chung, "Comparison of submicron-diameter carbon filaments and conventional carbon fibers as fillers in composite materials," *J. Carbon*, vol. 39, no. 8, pp. 1119-1125, Jul. 2001.

[27] X. Shui and D. D. L. Chung, "Submicron diameter nickel filaments and their polymer-matrix composites," *J. Mater. Sci.*, vol. 35, pp. 1773-1785, Apr. 2000.

[28] L. Li and D. D. L. Chung, "Electrical and mechanical properties of electrically conductive polyethersulfone composites," *J. Composites*, vol. 25, no. 3, pp. 215-224, Mar. 1994.

[29] X. Shui and D. D. L. Chung, "Submicron nickel filaments made by electroplating carbon filaments as a new filler material for electromagnetic interference shielding," *J. electron. mater.*, vol. 24, pp. 107-113, Feb. 1995.

[30] L. D. Cremar *et al.*, "Mechanical and electrical characterization of carbon nanofibers produced from

water soluble precursors," *J. Mater. Today Commun.*, vol. 7, pp. 134-139, Jun. 2016.
[31] M. Bayat *et al.*, "Electromagnetic interference shielding effectiveness of hybrid multifunctional Fe3O4/carbon nanofiber composite," *J. Polym.*, vol. 55, no. 3, pp. 936-943, Feb. 2014.
[32] X. Hong and D. D. L. Chung, "Carbon nanofiber mats for electromagnetic interference shielding," *J. Carbon*, vol. 111, pp. 529-537, Jan. 2017.
[33] Z. H. Abbas Alsalami, and F. H. Abbas, "Ultra-High-Performance Concrete with Micro-to Nanoscale Reinforcement," *ACI Mater. J.*, vol. 121, no. 2, pp. 73-92, Mar. 2024.
[34] L. A. Sbia, A. Peyvandi, P. Soroushian, and A. M. Balachandra, "Optimization of ultra-high-performance concrete with nano-and micro-scale reinforcement," *Cogent Eng.*, vol. 1, no. 1, Dec. 2014, Art. no. 990673.
[35] C. Caloz, and A. Sihvola, "Electromagnetic chirality, part 1: the microscopic perspective [electromagnetic perspectives]," *IEEE Antennas Propag. Mag.*, vol. 62, no. (1), pp. 58-71, Feb. 2020.
[36] C. Caloz, and A. Sihvola, "Electromagnetic chirality, part 2: the macroscopic perspective [electromagnetic perspectives]," *IEEE Antennas Propag. Mag.*, vol. 62, no. 2, pp. 82-98, Mar. 2020.
[37] S. A. Tretyakov *et al.*, "Analytical antenna model for chiral scatterers: comparison with numerical and experimental data," *IEEE Trans. Antennas Propag.*, vol. 44, no. 7, pp. 1006-1014, Jul. 1996.
[38] F. Guerin, P. Banneller, and M. Labeyrie, "Scattering of electromagnetic waves by helices and application to the modelling of chiral composites. I: Simple effective-medium theories," *J. Phys. D Appl. Phys.*, vol. 28. No. 4, pp. 623-642, Apr. 1995.
[39] F. Guerin, P. Bannelier, M. Labeyrie, J. P. Ganne, and P. Guillon, "Scattering of electromagnetic waves by helices and application to the modelling of chiral composites. II. Maxwell Garnett treatment," *J. Phys. D Appl. Phys.*, vol. 28, no. 4, pp. 643-656, Apr. 1995.
[40] A. Hamidi, A. Cheldavi, A. H. Korayem, "A lightweight concrete composite material with improved EMI shielding by using a chiral particle array," *AIP Advances*, vol 14, no. 8, Aug. 2024, Art. no. 085018.
[41] Y. Li *et al.*, "A new orientational molding method for ultra-high performance concrete with high content of steel fiber and investigation on its flexure and axial tensile properties," *J. Construction Building Mater.*, vol. 400, Oct. 2023, Art. no. 132755.
[42] H. Gou *et al.*, "Reinforcement mechanism of orientally distributed steel fibers on ultra-high-performance concrete," *J. Construction Building Mater.*, vol. 281, Apr. 2021, Art. no. 122646.
[43] J. Gong *et al.*, "Utilization of fibers in ultra-high performance concrete: A review," *J. Composites Part B Eng.*, vol. 241, Jul. 2022, Art. no. 109995.
[44] S. Zimmer, M. Helwig, A. Winkler, and N. Modler, "Modeling electrical conductivity of metal meshes for predicting shielding effectiveness in magnetic fields of wireless power transfer systems," *Electronics*, vol. 11, no. 14, Jul. 2022, Art. no. 2156.
[45] S. Y. Hyun *et al.*, "Modified sheet inductance of wire mesh using effective wire spacing," *IEEE Trans. Electromagn. Compat.*, vol. 58, no. 3, pp. 911-914, Mar. 2016.
[46] M. S. Sarto, S. Greco, and A. Tamburrano, "Shielding effectiveness of protective metallic wire meshes: EM modeling and validation," *IEEE Trans. Electromagn. Compat.*, vol. 56, no. 3, pp. 615-621, Jan. 2014.
[47] L. B. Wang *et al.*, "Electromagnetic shielding analysis of printed flexible meshed screens." In *IEEE Asia-Pacific Int. Symp. Electromagn. Compat.*, Beijing, China, 2010, pp. 965-968.
[48] V. M. Primiani, F. Moglie, and A. Pia Pastore, "Field penetration through a wire mesh screen excited by a reverberation chamber field: FDTD analysis and experiments," *IEEE Trans. Electromagn. Compat.*, vol. 51, no. 4, pp. 883-891, Oct. 2009.
[49] G. Lovat, P. Burghignoli, and S. Celozzi, "Shielding properties of a wire-medium screen, " *IEEE trans. Electromagn. Compat.*, vol. 50, no. 1, pp. 80-88, Feb. 2008).
[50] V. V. Yatsenko, S. A. Tretyakov, S. I. Maslovski, and A. A. Sochava, "Higher order impedance boundary conditions for sparse wire grids," *IEEE Trans. Antennas Propag.*, vol. 48, no. 5, pp. 720-727, May 2000.
[51] K. F. Casey, "Electromagnetic shielding behavior of wire-mesh screens," *IEEE trans. Electromagn. Compat.*, vol. 30, no. 3, pp. 298-306, Aug.1988).
[52] S. Celozzi, R. Araneo, and G. Lovat, "Frequency Selective Surfaces," in *Electromagnetic Shielding*, Hoboken, New Jersey, United States of America: John Wiley & Sons, 2008, chapter 10, pp. 219-240.

Ayoub Hamidi was born in Hamedan, Iran, in 1988. He received a B.Sc. degree in applied mathematics from the University of Qom, Qom, Iran, in 2012 and an M.Sc. degree in electrical engineering from the University of Tabriz, Tabriz, Iran, in 2016. He is currently pursuing a Ph.D. degree in communication engineering at the EMC Laboratory, Iran University of Science and Technology, Tehran. In 2016, he joined the EMC Laboratory, at the Iran University of Science and Technology. His research interests include electromagnetic compatibility, metamaterial, theoretical electromagnetics, Antenna design, and digital signal processing.

Ahmad Cheldavi was born in Ahwaz, Iran, in 1966. He received the B.Sc. degree (with honors) from the Iran University of Science and Technology (IUST), Tehran, Iran, in 1992, and the M.Sc. and Ph.D. degrees (with honors) from the School of Electrical Engineering, University of Tehran, Tehran, Iran, in 1994 and 2000, respectively. He is currently a Professor at the School of Electrical Engineering, IUST. At present, he also holds the position of President at Shahed University. He has authored over 100 journal and conference papers in the field of EMC/EMI and microwave transmission lines, genetic algorithms, and coupled line characterization.

Asghar Habibnejad Korayem received a B.Sc. degree in Structural Engineering from the School of Civil Engineering, Amirkabir University of Technology, Tehran, Iran, the M.Sc. degree from Tarbiat Modares University, Tehran, Iran, and the Ph.D. degree from Monash University, Melbourne, Australia. He is currently an Associate Professor at the Department of Civil Engineering at Iran University of Science and Technology (IUST), Tehran, Iran. His research interests include Nanotechnology application in civil engineering, Carbon nanotube-reinforced epoxy/cement/concrete composites, Graphene reinforced epoxy/cement/concrete composites, FRP Strengthening of Structures, Thin Steel shear walls, and Concrete technology.